Atmos. Chem. Phys. Discuss., 12, 3619–3653, 2012
www.atmos-chem-phys-discuss.net/12/3619/2012/
doi:10.5194/acpd-12-3619-2012

Atmospheric Chemistry and Physics Discussions

Signals of El Niño Modoki in the tropical tropopause layer and stratosphere

F. Xie[1], J. Li[1], W. Tian[2], and J. Feng[1]

[1]State Key Laboratory of Numerical Modeling for Atmospheric Sciences and Geophysical Fluid Dynamics, Institute of Atmospheric Physics, Chinese Academy of Sciences, Beijing, China
[2]Key Laboratory for Semi-Arid Climate Change of the Ministry of Education, College of Atmospheric Sciences, Lanzhou University, China

Received: 24 October 2011 – Accepted: 21 January 2012 – Published: 2 February 2012

Correspondence to: J. Li (ljp@lasg.iap.ac.cn)

Published by Copernicus Publications on behalf of the European Geosciences Union.

Abstract

The effects of El Niño Modoki events on the tropical tropopause layer (TTL) and on the stratosphere were investigated using European Center for Medium Range Weather Forecasting (ECMWF) reanalysis data, satellite observations from the Aura satellite Microwave Limb Sounder (MLS), oceanic El Niño indices, and general climate model outputs. El Niño Modoki events tend to depress convective activities in the western and eastern Pacific but enhance convective activities in the central and northern Pacific. Consequently, during Modoki events, negative water vapor anomalies occur in the western and eastern Pacific upper troposphere, whereas there are positive anomalies in the central and northern Pacific upper troposphere. The spatial patterns of the outgoing longwave radiation (OLR) and upper tropospheric water vapor anomalies exhibit a tripolar form. The empirical orthogonal function (EOF) analysis of the OLR and upper tropospheric water vapor anomalies reveals that canonical El Niño events are associated with the leading mode of the EOF, while El Niño Modoki events correspond to the second mode. El Niño Modoki activities tend to moisten the lower and middle stratosphere, but dry the upper stratosphere. It was also found that the canonical El Niño signal can overlay linearly on the QBO signal in the stratosphere, whereas the interaction between the El Niño Modoki and QBO signals is non-linear. Because of these non-linear interactions, El Niño Modoki events have a reverse effect on high latitudes stratosphere, as compared with the effects of typical Modoki events, i.e. the northern polar vortex is stronger and colder but the southern polar vortex is weaker and warmer during El Niño Modoki events. However, simulations suggest that canonical El Niño and El Niño Modoki activities actually have the same influence on high latitudes stratosphere, in the absence of interactions between QBO and ENSO signals. The present results also reveal that canonical El Niño events have a greater impact on the high-latitude Northern Hemisphere stratosphere than on the high-latitude Southern Hemisphere stratosphere. However, El Niño Modoki events can more profoundly influence the high-latitude Southern Hemisphere stratosphere than the high-latitude Northern Hemisphere stratosphere.

ACPD
12, 3619–3653, 2012

1 Introduction

The El Niño-Southern Oscillation (ENSO) is an important signal of interannual variability in the atmosphere. It can impact the troposphere by adjustment of convection patterns and can influence the stratosphere through the anomalous propagation and dissipation of ultralong Rossby waves at middle latitudes. The two reversal phases of the ENSO cycle are (1) a "warm" phase (called El Niño), in which an anomalously warm tongue of sea surface water spreads westward from the eastern Pacific Ocean to the middle and western Pacific Ocean; and (2) a "cold" phase (called La Niña), in which a broad anomalously cold tongue of sea surface water in this region.

These two phases result in dramatically different patterns of atmospheric convection throughout the tropical atmosphere (Philander, 1990), i.e. the warm phase enhances convection in the middle and eastern tropical Pacific, but depresses convection in the western tropical Pacific, while the cold phase has the effect of weakening convection in the middle and eastern tropical Pacific but enhancing convection in the western tropical Pacific. These patterns can affect the properties of the TTL, including temperatures, wind velocities, and water vapor and ozone concentrations (Chandra et al., 1998; Gettelman et al., 2001; Kiladis et al., 2001; Newell et al., 1996; Randel et al., 2000; Reid and Gage, 1985; Sassi et al., 2004; Yulaeva and Wallace, 1994), which, in turn, can influence stratospheric water vapor concentrations (e.g. Gettelman et al., 2001; Sassi et al., 2004; Scaife et al., 2003). In addition, previous studies have indicated that warm phases of the ENSO can significantly enhance planetary wave activities (Van Loon and Labitzke, 1987; Hamilton, 1993; Camp and Tung, 2007; Garfinkel and Hartmann, 2007; Free and Seidel, 2009; Sassi et al., 2004; Manzini et al., 2006; García-Herrera et al., 2006; Taguchi and Hartmann, 2006), resulting in stronger stratospheric Brewer-Dobson (BD) circulation. Cagnazzo et al. (2009), on the basis of the results of several atmospheric chemistry climate models, and Free and Seidel (2009), on the basis of observations, both reported a warming of the northern polar vortex during strong warm phases of the ENSO, associated with increased ozone anomalies in northern high latitudes.

ACPD
12, 3619–3653, 2012

Using tropical Pacific Ocean sea surface temperatures (SST), the canonical El Niño pattern can be derived from the first mode of an EOF analysis (e.g. Rasmusson and Carpenter, 1982; Trenberth, 1997; Zhang et al., 2009), showing maximum sea surface temperature anomalies (SSTA) in the eastern Pacific (Fig. 1a). However, the second mode of tropical Pacific Ocean SST variability depends on the study period of the data series. For example, EOF analyses performed on tropical Pacific SSTA at time scales close to or greater than 50 yr (e.g. 1948–2007 and 1880–2007) yield a cooling mode in the equatorial Pacific cold tongue (Zhang et al., 2010). However, for the time series from 1979 to 2004, the second mode of the EOF, which accounts for approximately 12 % of the total variance, shows a warm SSTA located in the central tropical Pacific (Ashok et al., 2007). This mode, referred to as El Niño Modoki, corresponds to the third mode of the EOF analysis of long-term SSTA (e.g. 1948–2007 and 1880–2007) over the tropical Pacific (Zhang et al., 2010), which shows negative SSTAs in the eastern and western Pacific, and positive SSTA in the central Pacific (Fig. 1b).

Ashok et al. (2007) found that the evolution of El Niño Modoki events is related to a tripolar pattern of sea level pressure anomalies, and noted the presence of two anomalous Walker circulation cells associated with El Niño Modoki events, versus the single cell that is associated with canonical El Niño events. This configuration of atmospheric circulation in El Niño Modoki events appears to influence the troposphere in a different way than that of canonical El Niño events. Weng et al. (2007, 2009) assessed the impact of El Niño Modoki events on the climate of China, Japan, and the United States, during the boreal summer and winter, on the basis of data from three El Niño Modoki events. They found that El Niño Modoki activities influence climate in a different way to that of canonical El Niño activities. Recently, The modulation of SSTA on convection, and the resulting effects of El Niño Modoki events on regional rainfall, have received considerable attention (Taschetto and England, 2009; Cai and Cowan, 2009; Feng and Li, 2011; Zhang et al., 2011). Those studies indicate that the two types of El Niño (canonical El Niño and El Niño Modoki) show contrasting impacts on regional rainfall patterns. On the one hand, both Walker circulation patterns and the effects of

ACPD
12, 3619–3653, 2012

convection anomalies caused by El Niño Modoki activities can extend to the TTL. On the other hand, the gradient patterns of SSTA of canonical El Niño and El Niño Modoki events would be associated with distinctly different patterns of propagation and dissipation of ultralong Rossby waves in the mid-latitude stratosphere, which may lead to profoundly different effects on the stratosphere. Trenberth and Smith (2006, 2009) have noted distinct temperature anomalies in the stratosphere caused by the two types of El Niño activities, although the possible relationships between the temperature changes and wave activities or circulation anomalies were not discussed in their study.

The influence of warm vs. cold phases of the ENSO on the atmosphere has been carefully investigated in the past, whereas the atmospheric response to El Niño Modoki events, especially in the TTL and stratosphere, has not to receive sufficient attention. This study investigates the effects of El Niño Modoki activities on the TTL and stratosphere, and compared those effects with those of canonical El Niño activities. The remainder of the manuscript is organized as follows. Section 2 describes the data used in the study and related numerical simulations. Section 3 discusses how patterns of atmospheric convection, the tropopause temperature, and water vapor changes in the upper troposphere and tropopause, are related to the activities of the two types of El Niño. Section 4 analyses variations in stratospheric water vapor, wave activities, and circulation and temperature patterns associated with the two types of El Niño activities. Finally, the conclusions are presented in Sect. 5.

2 Data and simulations

The data used in the present study include outgoing longwave radiation (OLR), tropopause temperature, water vapor concentration, and wind field data. The OLR data from 1979 to 2010 were obtained from http://www.cdc.noaa.gov/. The monthly mean European Center for Medium Range Weather Forecasting (ECMWF) reanalysis data (ERA-Interim) from 1979 to 2010 were analyzed mainly for tropopause temperatures, tropospheric water vapor concentrations, and stratospheric wind fields and

ACPD
12, 3619–3653, 2012

temperatures. The ERA-Interim data assimilates new model outputs and satellite observations, and provide data at horizontal resolutions of $1.5 \times 1.5^{\circ}$ and relatively high vertical resolutions (Simmons et al., 2007a, b; Uppala et al., 2008). The ERA-Interim data are therefore suitable for diagnosing water vapor concentrations and temperature anomalies in the TTL, and wind fields and temperatures in the stratosphere. Because the stratospheric water vapor concentration data in the ERA-Interim database may be systematically biased with respect to actual values (Gettelman et al., 2010), the data from the Microwave Limb Sounder (MLS) on the AURA satellite are used for stratospheric water vapor analysis.

The monthly Nino 3 index (5° N–5° S, 150–90° W), hereafter N3I, and the ENSO Modoki index, hereafter EMI, were used to identify monthly occurrences of canonical El Niño events and El Niño Modoki events, respectively. N3I is defined as the area mean SSTA over the region 5° S–5° N, 150–90° W, and is available at http://www.cpc.noaa.gov/data/indices/. Following Ashok et al. (2007), the EMI is defined as follows:

$$\mathrm{EMI} = [\mathrm{SSTA}]_{\mathrm{C}} - 0.5 \cdot [\mathrm{SSTA}]_{\mathrm{E}} - 0.5 \cdot [\mathrm{SSTA}]_{\mathrm{W}}$$

where the subscripted brackets represent the area mean SSTA over the central Pacific region ($[\mathrm{SSTA}]_{\mathrm{C}}$: 10° S–10° N, 165° E–140° W), the eastern Pacific region ($[\mathrm{SSTA}]_{\mathrm{E}}$: 15° S–5° N, 110–70° W), and the western Pacific region ($[\mathrm{SSTA}]_{\mathrm{W}}$: 10° S–20° N, 125–145° E). Months with canonical El Niño event were identified by the corresponding N3I values equal to or greater than +0.5°C in those months. Similarly, months with El Niño Modoki events were identified by the corresponding EMI values equal to or greater than +0.5°C. The NOAA OLR, ERA-Interim, and MLS data were divided into two groups on the basis of the N3I and EMI data. Group one contains data recorders marked with canonical El Niño events. Group two contains data recorders marked with El Niño Modoki events. The canonical El Niño and El Niño Modoki anomalies are calculated using composites of the detrended and deseasonalized time series for canonical El Niño and El Niño Modoki events, respectively. Note that the MLS dataset from 2005 to 2010 contains only one time characteristic of typical El Niño processes (durations

ACPD
12, 3619–3653, 2012

of 6 month) and one time characteristic of El Niño Modoki processes (durations of 6 month). Although small numbers of events identified over relatively short time intervals may not be representative of long-term climatological patterns, the analysis of MLS stratospheric water vapor data provides more robust results than can be obtained using ERA-interim data, even though the latter span a longer period of time.

Our composite results, based on reanalysis data and observations, were also compared with time-slice simulations derived from the Whole Atmosphere Community Climate Model, version 3 (WACCM3), using forcing of observed canonical El Niño and El Niño Modoki SSTs from the tropical Pacific. The WACCM3, provided by the National Center for Atmospheric Research (NCAR; http://cdp.ucar.edu/), is unable to internally simulate quasi-biennial oscillation (QBO) signals; however, it can rationally simulate atmospheric ENSO signals (Garcia et al., 2007). The WACCM3 has 66 vertical levels extending from the ground to 4.5×10^{-6} hPa (~145 km geometric altitude), and the model's vertical resolution is 1.1–1.4 km in the TTL and the lower stratosphere (<30 km). The three time-slice simulations presented in this paper were performed at a resolution of $1.9 \times 2.5^{\circ}$, with interactive chemistry disabled. The three runs were conducted with configurations using the same greenhouse gas (GHG) emissions but different SST forcing. The SST used in the control experiment (R1) is observed monthly mean climatology for the time period from 1979 to 2010. In experiment R2, SST is as in R1, except that the tropical Pacific SST represents composite of observed SST associated with canonical El Niño conditions, for the period 1979–2010. In experiment R3, the SST is as in R1, but the tropical Pacific SST represents composite of observed SST associated with El Niño Modoki conditions. The observed SST data is from the Meteorological Office, Hadley Centre for Climate Prediction and Research, SST and sea-ice field datasets (Rayner et al., 2006). The averaged differences of SSTs in the tropical Pacific between sensitive experiments and the control experiment (R2-R1 and R3-R1) are similar with the SSTAs in Fig. 1a and b. The fixed GHG values used in the model radiation scheme are based on emissions scenario A2 of the Intergovernmental Panel on Climate Change (IPCC) (WMO, 2003), averaged GHG values for the period

ACPD
12, 3619–3653, 2012

1979–2010. All experiments were ran for 18 yr with the first 3 yr excluded for the model spin-up and only the remaining 15 yr are used for the analysis. The model climatologies are based on the last 15 yr of the model output except when otherwise stated.

3 Anomalies in the TTL associated with the two types of El Niño

Changes in SST cause profound changes in atmospheric convection. In this paper, the magnitude of OLR is used as a proxy for the intensity of convective activity. Figure 2 shows OLR anomalies associated with canonical El Niño and El Niño Modoki events. It is evident that typical El Niño phases have different impacts on convection patterns in different tropical regions, i.e. enhanced convection (negative OLR anomalies) occurs in the middle and eastern Pacific during canonical El Niño events, while reduced convection (positive OLR anomalies) occurs in the western and northern Pacific (Fig. 2a). The spatial patterns and magnitudes of the OLR anomalies exhibited in Fig. 2a are similar to those reported in previous studies (e.g. Philander, 1990; Deser and Wallace, 1990; Yulaeva and Wallace, 1994; Kiladis et al., 2001; Gettelman et al., 2001).

Using regression analysis, Trenberth and Smith (2009) pointed out that the OLR signatures of the two types of El Niño are quite similar. However, it was found that the composite anomalies of convective activities associated with El Niño Modoki events (Fig. 2b) are somewhat different from those associated with canonical El Niño events (Fig. 2a). El Niño Modoki events depress convection in the western and eastern Pacific but intensify convection in the central and northern Pacific. In addition, the positive and negative anomalies over the middle and western Pacific, respectively, during El Niño Modoki are weaker than those associated with canonical El Niño events. Furthermore, the OLR anomalies show a tripolar form as SSTA during El Niño Modoki events, with patterns that correspond to patterns of rainfall anomalies, as noted by Ashok et al. (2007) and Weng et al. (2009).

The EOF analysis of deseasonalized and detrended monthly mean OLR anomalies, for the period 1979–2010, can effectively isolate El Niño variability. The leading mode, which explains 16 % of the variance of EOF spatial patterns, is similar to the canonical

ACPD
12, 3619–3653, 2012

El Niño pattern of OLR anomalies (Fig. 2a and c). The interannual variability of the leading mode of EOF time patterns (Principal Component, PC) (Fig. 2e, black line) and the N3I (Fig. 2e, red line) are strongly correlated (linear correlation coefficient, 0.75). This result is in agreement with the results of previous studies (Gettelman et al., 2001; Kiladis et al., 2001). Gettelman et al. (2001) noted that the second mode of the EOF analysis of OLR anomalies is also statistically significant, explaining about 8 % of the variance of EOF spatial patterns, and maps strongly onto the central and western Pacific. They further note that the second mode is similar to a second ENSO mode (the "Trans-Niño Index") described by Trenberth and Stepaniak (2001). Figure 2d and f show EOF spatial patterns and interannual variabilities of PC corresponding to the second mode of EOF analysis. The results show that the EOF spatial pattern corresponds to OLR anomalies during El Niño Modoki events (Fig. 2b and d), and the PC mode is strongly correlated with the EMI (Fig. 2f, black and red lines) (linear correlation coefficient, 0.60). This finding indicates that the second mode of the OLR anomalies corresponds with the Modoki pattern, as noted by Gettelman et al. (2001).

The patterns of OLR anomalies of the two types of El Niño can also be obtained from the WACCM3 forced by observed SSTA (Fig. 3). Figure 3a and b show the OLR differences between run R2 and R1 and between run R3 and R1, respectively. The patterns of OLR anomalies generated by the WACCM3 are broadly similar to the composited results of observations (Figs. 2a and b; 3a and b). However, in the observations, the maximum OLR anomaly that is located over the Maritime Continent migrates to the north Pacific in the model, and in the Indian Ocean, negative anomalies in observed OLR values change to positive anomalies in the model results. The discrepancies between observations and NCAR model outputs have also been noted by Gettelman et al. (2001).

In summary, the above analysis shows that El Niño Modoki activities have a significantly different influence on the troposphere than do typical El Niño activities. Separating the effects of El Niño Modoki activities and canonical El Niño activities is critical for considering the impacts of El Niño activities on the atmosphere.

ACPD
12, 3619–3653, 2012

It is well known that changes in convection patterns can profoundly affect tropical circulation. Variations in convection and circulation patterns resulting from SSTA have been shown to significantly influence tropopause temperatures (Reid and Gage, 1985). These patterns of change can be confirmed at several levels in the TTL. Here, the composite anomalies of 100 hPa temperatures associated with canonical El Niño and El Niño Modoki events are analyzed, based on ERA-Interim data from 1979 to 2010 (Fig. 4). The results indicate cooling in the middle and eastern Pacific at 100 hPa during canonical El Niño events, while in the western Pacific region, where typically referred to as the "cold trap region" (Newell and Gould-Stewart, 1981), the 100 hPa temperature shows a warming exceeding 1.0 K (Fig. 4a). The spatial patterns and magnitudes of the temperature anomalies exhibited in Fig. 4a are in agreement with the results of previous studies (e.g. Randel et al., 2000; Scaife et al., 2003; Xie et al., 2011). Figure 4a shows that 100 hPa temperature signals of canonical El Niños is opposite to that of tropical SST. Previous studies have shown that the sign of the El Niño signal is opposite to that of the tropical lower stratosphere (Reid et al., 1989; Yulaeva et al., 1994). Calvo et al. (2004) suggested that cooling of the tropical lower stratosphere over the eastern Pacific during warm phases of ENSO is related to internal equatorial waves associated with SSTA that force anomalous convection in the troposphere. Although Fig. 2 shows differences in the convection patterns of canonical El Niño and El Niño Modoki events, the patterns of 100 hPa temperature anomalies in the two types of El Niño events are similar; this result is in agreement with the results of Trenberth and Smith (2009). However, the 100 hPa temperature anomalies are smaller in El Niño Modoki events than in canonical El Niño events (Fig. 4a and b). This phenomenon is further confirmed by WACCM3 simulations (Fig. 4c and d), implying that the internal equatorial waves, which affect tropopause temperature anomalies during ENSO periods, may be mainly motivated by the SSTAs in the equatorial western and middle Pacific, as patterns of SSTAs in these two regions during canonical El Niño and El Niño Modoki events are the same (Fig. 1). Because the SSTA gradient between the middle and western Pacific during El Niño Modoki events is weaker than that observed during canonical El Niño

ACPD
12, 3619–3653, 2012

events, the corresponding tropopause temperature anomalies are also smaller (Fig. 4).

Figure 5 shows the cold point tropopause temperature anomalies associated with the two types of El Niño events. Here, the cold point tropopause is determined as the pressure level in the upper troposphere and lower stratosphere that has the lowest temperature. Figure 5 shows that the distributions and magnitudes of cold point tropopause temperature anomalies are similar to those of 100 hPa temperature anomalies.

A variety of processes govern water vapor concentrations in the TTL (see chapter 3 in SPARC, 2000). In the upper troposphere, water vapor concentrations are strongly correlated with convective activity (Chandra et al., 1998; Gettelman et al., 2001; McCormack et al., 2000; Newell et al., 1996). In the tropopause layer, temperature is a principal factor controlling water vapor changes, via freeze-drying processes (Brewer, 1949; Holton et al., 1995). Thus, changes in convection patterns and tropopause temperature during the two types of El Niño periods are likely linked with water vapor changes. In the subsequent paragraph, water vapor anomalies in the TTL during canonical El Niño and El Niño Modoki events are discussed, using ERA-Interim data, which may help to clarify patterns of stratospheric water vapor change during these two types of events.

Figure 6 shows upper tropospheric (250 hPa) water vapor anomalies for the two types of El Niño events. The data indicate that canonical El Niño activities significantly moisten the upper troposphere in the middle and eastern Pacific and the Indian Ocean (Fig. 6a), but dry the upper troposphere over the western Pacific and the Maritime Continent. This finding is consistent with observations of single El Niño events (Newell et al., 1996; Chandra et al., 1998; Gettelman el al., 2001). The upper tropospheric water vapor anomalies during El Niño Modoki periods show a different pattern from those of canonical El Niño periods. The locations of the maximum water vapor anomalies shift westward (Fig. 6b), and a negative anomaly is observed over the eastern Pacific. The magnitudes of positive and negative anomalies over the central Pacific and the Maritime Continent, respectively, during El Niño Modoki events are reduced, as compared with the anomalies associated with canonical El Niño events. The anomaly patterns in

ACPD
12, 3619–3653, 2012

Fig. 6a and b resemble the OLR patterns during canonical El Niño and El Niño Modoki phases (Fig. 2a and b), respectively. That is, upper troposphere humidity anomalies are correlated with convection patterns. In addition, the EOF analysis revealed that the leading mode of the 250 hPa water vapor anomalies is associated with canonical El Niño patterns, while the second mode is associated with El Niño Modoki patterns (Not shown). Figure 6c and d shows the 250 hPa water vapor anomalies in the two types of El Niño events obtained by the simulations from WACCM3 forced with observed SSTA. The model results are in good agreement with observations in the Pacific region. However, in the Indian Ocean a negative water vapor anomaly can be noted in simulations which is different from observations (Figs. 6c and d; a and b).

Figure 7 shows water vapor anomalies in the two types of El Niño events at 100 hPa. The anomalies during canonical El Niño events (Fig. 7a) are generally consistent with temperature anomalies (Fig. 4a), i.e. negative and positive temperature anomalies are associated with negative and positive water vapor anomalies, respectively. As expected, patterns of water vapor anomalies in El Niño Modoki events are similar to those of canonical El Niño events (Fig. 7a and b); this is related to the fact that the two types of El Niño cause similar patterns of 100 hPa temperature anomalies (Fig. 4a and b). Similarly, the 100 hPa water vapor anomalies in El Niño Modoki events are smaller than those observed in canonical El Niño events; this is related to that the two types of El Niño cause different degree of anomalies of 100 hPa temperature. These results are confirmed by WACCM3 simulations (Fig. 7c and d).

4 El Niño Modoki signals in the stratosphere

The entry of water vapor into the lower stratosphere is controlled mainly by the tropopause temperature. Figures 4 and 5 show large spatial variations in the effect of two types of El Niño events on tropopause temperature. To estimate the net effects of the two types of El Niño events on stratospheric water vapor concentrations, the averaged vertical profiles of composite zonal mean water vapor anomalies in the tropics

ACPD
12, 3619–3653, 2012

(25° S–25° N) are discussed (Fig. 8); these data represent observational water vapor data from the MLS measurements (2005–2010), as the assimilated stratospheric water vapor data from the ERA-Interim database may contain systematic biases as compared with actual observations (Gettelman et al., 2010). It is also worth noting that water vapor data from the National Aeronautics and Space Administration's (NASA's) Halogen Occultation Experiment (HALOE) and Stratospheric Aerosol and Gas Experiment (SAGE), which spans a longer time period, may be more suitable for composite analyses. However, due to excessive numbers of missing values in the HALOE and SAGE datasets in the tropical stratosphere, the MLS dataset is analyzed, which spans a relatively short period of time but contains more complete monthly data values. In addition, it was still able to obtain composite anomalies for both canonical El Niño and El Niño Modoki events for the 6-yr time period of interest, thereby deriving more evidence regarding ENSO's effects on stratospheric water vapor.

Figure 8 shows that canonical El Niño activities result in positive water vapor anomalies in the tropical lower stratosphere, which is consistent with the findings of previous studies, i.e. El Niño events have a moistening impact on the lower stratosphere (e.g. Fueglistaler and Haynes, 2005; Gettelman et al., 2001; Geller et al., 2002; Hatsushika and Yamazaki, 2003), and in the upper stratosphere, but tend to dry the tropical middle stratosphere (Xie et al., 2011). El Niño Modoki activities moisten the tropical lower stratosphere but they also moisten the middle stratosphere, and dry the upper stratosphere. Xie et al. (2011) pointed out that middle stratospheric water vapor anomalies are influenced mainly by tropopause temperature anomalies over the middle and eastern Pacific during ENSO periods. The foregoing analysis illustrates that during El Niño Modoki events, the negative tropopause temperature anomalies over the middle and eastern Pacific are substantially weaker than those related to canonical El Niño events (Figs. 4 and 5). Thus, the negative anomalies over the middle and eastern Pacific related to El Niño Modoki events cannot substantially influence the middle stratosphere, as is the case for canonical El Niño events.

ACPD
12, 3619–3653, 2012

The different SST-gradient patterns associated with canonical El Niño and El Niño Modoki events is likely to lead to the anomalous propagation and dissipation of ultralong Rossby waves in the stratosphere, which would cause profound and distinct stratospheric circulation anomalies. This section considers the effects of the two types of El Niño activities on circulation in the stratosphere, beginning with an analysis of the changes in Eliassen-Palm (E-P) fluxes (Eliassen and Palm, 1961; Andrew et al., 1987). E-P fluxes which represent wave activities related to the strengths of BD circulation and zonal mean flow, have been applied to analyze planetary wave propagation in previous studies (e.g. Randel, 1987; Hu and Tung, 2002; Hitoshi and Hirooka, 2004). An expression to calculate the E-P flux was given by Andrew et al. (1987). The meridional and vertical components of the E-P flux are, respectively:

$$F_y = -\rho_o a(\cos\phi)\overline{v'u'}$$

$$F_z = \rho_o a(\cos\phi) f \overline{v'\theta'}/\theta_{0z},$$

where ρ_o is the density of background air, θ is the potential temperature, a is the radius of the earth, v is the mean meridional wind, and ω is the mean vertical velocity in pressure units. The subscript z denotes derivatives with respect to height z. The overbar denotes the zonal mean and the accent denotes deviations from the zonal mean.

Figure 9 shows anomalies of the E-P flux, zonal wind, and temperature induced by two types of El Niño activities. Figure 9a demonstrates that canonical El Niño events increase the upward propagation of wave activity in the polar stratosphere in the Northern Hemisphere mid-latitudes, which suggests a strengthening of BD circulation in the Northern Hemisphere. Consequently, the northern polar vortex is weakened and warmed (Fig. 9a and b). These results are consistent with those of previous studies, showing that BD circulation in the Northern Hemisphere is enhanced during El Niño events (Manzini et al., 2006; Garfinkel and Hartmann, 2007; Free and Seidel, 2009), and that a warming of the northern polar vortex occurs during strong warm phases of

ACPD
12, 3619–3653, 2012

ENSO can be found in both simulation (Cagnazzo et al., 2009) and observation (Free and Seidel, 2009). However, a significant decrease in wave activity in the Southern Hemisphere stratosphere suggests diminished BD circulation during canonical El Niño events, which is conductive to an increase in zonal winds in mid-latitudes stratosphere. Figure 9 also shows that canonical El Niño activities have no significant impact on the strength of the southern polar vortex; however, cooling is apparent in the southern polar vortex (Fig. 9a and b), which may be a result of decreased ozone transport from the tropical stratosphere to the Southern Hemisphere high-latitude stratosphere, and weakened adiabatic compression in the southern polar vortex because of weakened BD circulation during canonical El Niño events in the Southern Hemisphere.

It is interesting that the anomalies in wave activity, zonal wind, and temperature during El Niño Modoki events are, overall, different from those during canonical El Niño events. El Niño Modoki events cause a significant increase in wave activity in Southern Hemisphere mid-latitude regions, which depresses and warms the southern polar vortex (Fig. 9c and d). El Niño Modoki activities have a relatively weak effect on the Northern Hemisphere high-latitude stratosphere; they suppress the upward propagation of wave activity, which corresponds to a stronger and colder northern polar vortex.

The results in Fig. 9 imply that canonical El Niño events have a more significant impact on the high-latitude Northern Hemisphere stratosphere than they do on the high-latitude Southern Hemisphere stratosphere. Nevertheless, El Niño Modoki events can more profoundly influence the high-latitude Southern Hemisphere stratosphere than the high-latitude Northern Hemisphere stratosphere.

In a regression analysis using Japanese Reanalysis (JRA-25) and 40-yr European Centre for Medium-Range Weather Forecasts Re-Analysis (ERA-40) datasets, Trenberth and Smith (2006 and 2009) noticed different stratospheric temperatures corresponding to the two types of El Niño events. These anomalies can also be reproduced by general climate model simulations (Zhou et al., 2010). Through a composite analysis using a variety of reanalysis data, Hurwitz et al. (2011) also found a warming effect of El Niño Modoki events on the southern polar vortex, and they further noted that the

ACPD
12, 3619–3653, 2012

enhancement of wave activity in the Southern Hemisphere contributes to the easterly phase of the QBO during El Niño Modoki events. Note that significant zonal wind and temperature anomalies in the tropical stratosphere corresponding to the two types of El Niño events (Fig. 9a and b) should also be related to the QBO (García-Herrera et al., 2006); however, the anomalies in El Niño Modoki events show diverse patterns as compared with those of typical El Niño events. That is, positive and negative anomalies in upper stratosphere zonal winds are of typical El Niño and El Niño Modoki periods, respectively, and positive and negative anomalies in lower stratosphere temperatures are of typical El Niño and El Niño Modoki periods, respectively. These observations indicate that the QBO signal affects the signals of the two types of El Niño in the tropical stratosphere in different ways, perhaps as a distinct linear overlay of QBO and ENSO signals on the two types of El Niño.

Figure 10 shows anomalies in E-P fluxes, zonal winds, and temperature obtained by the WACCM3, forced with observed SSTAs in the typical El Niño and El Niño Modoki events. The model results for the effects of canonical El Niño activities on mid-high latitudes stratospheric wave activity, circulation, and temperature are consistent with the composite results obtained using reanalysis data; however, in the tropical stratosphere, the anomalies obtained using the model are different from those obtained using the reanalysis data (Figs. 10a and b; 9a and b). Because the present simulations were unable to internally simulate QBO signals, the model cannot reproduce actual tropical stratospheric zonal wind anomalies during typical El Niño periods. The simulation also confirms the result from Garfinkel and Hartmann (2007) that, excluding stratospheric QBO signal, ENSO warm phase does have a significant effect on the polar vortex. Surprisingly, the simulated E-P fluxes, zonal winds, and temperature anomalies forced by El Niño Modoki SSTA are similar to the simulated results forced by typical El Niño SSTA (Fig. 10a and d). The model outputs of the present study support the views of Hurwitz et al. (2011), because the present simulations lack the impact of the QBO signal on El Niño Modoki activities, the model cannot accurately reproduce the effects of El Niño Modoki activities on stratospheric wave propagation in either hemisphere.

ACPD
12, 3619–3653, 2012

However, the simulated results suggest that the QBO signal is an important influence, not only on the El Niño Modoki signal in Southern Hemisphere stratospheric circulation, as pointed out by Hurwitz et al. (2011), but also on the El Niño Modoki signal in Northern Hemisphere stratospheric circulation. In addition, these results imply that typical El Niño and El Niño Modoki activities actually have the same influences on mid-high latitudes stratosphere when without the disturbance of the QBO signal on the ENSO signal.

It is interesting to note that, if QBO signals are filtered out of the composite zonal wind anomaly data obtained from the ERA-Interim time series dataset using the 24–40 months band-pass filter (as in Pascoe et al., 2005), the resulting zonal wind anomalies are virtually identical to those obtained for canonical El Niño periods using the WACCM3 forced by observed SSTA (Fig. 10a and 11a). However, the zonal wind anomalies obtained from filtered ERA-Interim time series data for El Niño Modoki periods are unlike the anomalies obtained using the WACCM3 forced by observed SSTA (Fig. 10c and 11b), they are still associated with the zonal wind anomalies obtained from the original ERA-Interim time series dataset for the high-latitude stratosphere (Fig. 9c and 11b). The present results reveal that anomalies in stratospheric zonal winds during El Niño Modoki periods are not simply a linear overlay of the QBO and ENSO signals, as is observed in canonical El Niño periods; therefore, there should be an interaction between the QBO signal and El Niño Modoki activities. Calvo et al. (2009) suggested that a possible mechanism for this interaction is the shift of zonal winds phase caused by QBO affects the propagation and dissipation of ultra-long Rossby waves in the stratosphere during warm ENSO events.

To further confirm the interaction between QBO and El Niño Modoki signals, we perform other two sensitive experiments, R4 and R5. The configurations of R4 are same as R2 but observed QBO phase signals from 1991 to 2005 (15 yr) included in WACCM3 as an external forcing for zonal wind. The configurations of R5 are same as R3 but observed QBO phase signals from 1991 to 2005 (15 yr) were included. It is found that zonal wind anomalies in R4 (R4-R1, Fig. 11c) is identical with the anomalies

ACPD
12, 3619–3653, 2012

in Figs. 9a and 10a in the mid-high latitudes stratosphere. However, we found the zonal anomalies in R5 (R5-R1, Fig. 11d) is consistent with Fig. 9c but completely different from Fig. 10c in the mid-high latitudes stratosphere. The results verify that due to the interaction between QBO and El Niño Modoki signals, the phase of mid-high latitudes stratospheric zonal wind anomalies in El Niño Modoki periods is opposite to that in typical El Niño periods.

5 Summary and conclusions

We investigated and compared the potential effects of the two types of El Niño events (canonical El Niño and El Niño Modoki) on the TTL and stratosphere, using composite analyses of ERA-Interim reanalysis data, based on the N3I and the EMI. As was found in earlier studies, the present results show that canonical El Niño events tend to enhance convection in the middle and eastern Pacific and weaken convection over the western Pacific. El Niño Modoki events, on the other hand, depress convection in the western and eastern Pacific and intensify convection in the central and northern Pacific; this leads to negative anomalies of upper tropospheric water vapor in the western and eastern Pacific but positive anomalies in the central and northern Pacific. These patterns of OLR and upper tropospheric water vapor anomalies caused by El Niño Modoki events correspond with a tripolar form. In addition, the positive and negative convection anomalies associated with El Niño Modoki events in the middle and western Pacific, respectively, are smaller than those associated with canonical El Niño events. An EOF analysis of the OLR and upper tropospheric water vapor anomalies demonstrates that the leading mode is a result of canonical El Niño events, and that the second mode is a result of El Niño Modoki events. El Niño activities lead to similar patterns of tropopause temperature and water vapor anomalies as those of canonical El Niño activities, although the El Niño Modoki anomalies are smaller than those of canonical El Niño events. The above results are also supported by general climate model simulations.

ACPD
12, 3619–3653, 2012

We also found that the two types of El Niño activities have significantly different effects on the stratosphere. As in previous studies, it was found that canonical El Niño activities result in positive water vapor anomalies (i.e. moistening) in the tropical lower stratosphere and upper stratosphere, but tend to dry the tropical middle stratosphere. El Niño Modoki activities also moisten the lower stratosphere (similar to El Niño activities), but moisten the middle stratosphere and dry the upper stratosphere. The stratospheric water vapor anomalies for the two types of El Niño events were derived on the basis of relatively short-duration datasets, and confirmation of the results requires analyses using longer-duration and more reliable time-series data.

We also found that the effects of the QBO signal on the stratosphere during El Niño events represent a simple linear overlay of the QBO and canonical El Niño signals, whereas there is a complex interaction between the QBO and El Niño Modoki signals. Because of this interaction, El Niño Modoki events have a reverse effect on stratospheric circulation at high latitudes, as compared with that of canonical Modoki events. During El Niño Modoki events, the northern polar vortex is stronger and colder but the southern polar vortex is weaker and warmer. However, the simulations suggest that canonical El Niño and El Niño Modoki activities actually have the same influence on high latitudes stratosphere, in the absence of interactions between QBO and ENSO signals. Finally, the present results suggest that canonical El Niño events have a more significant impact on the high-latitude Northern Hemisphere stratosphere than on the high-latitude Southern Hemisphere stratosphere. However, El Niño Modoki events more profoundly influence the high-latitude Southern Hemisphere stratosphere than they do the high-latitude Northern Hemisphere stratosphere.

Acknowledgements. This work was jointly supported by the 973 Program (2010CB950400) and 973 Program (2010CB428604) and the National Natural Science Foundation of China (41030961). W. T. thanks ECMWF for meteorological data and NOAA for OLR and ONI data as well as MLS data team for support. The WACCM model is provided by NCAR.

ACPD
12, 3619–3653, 2012

References

Ashok, K., Behera, S., Rao, S., Weng, H., and Yamagata, T.: El Niño Modoki and its teleconnection, J. Geophys. Res., 112, C11007, doi:10.1029/2006JC003798, 2007.

Andrews, D. G., Holton, J. R., and Leovy, C. B.: Middle Atmosphere Dynamics, Academic Press Inc., 489 pp., 1987.

Brewer, A. W.: Evidence for a world circulation provided by the measurements of helium and water vapour distribution in the stratosphere, Q. J. Roy. Meteorol. Soc., 75, 351–363, 1949.

Cagnazzo, C., Manzini, E., Calvo, N., Douglass, A., Akiyoshi, H., Bekki, S., Chipperfield, M., Dameris, M., Deushi, M., Fischer, A. M., Garny, H., Gettelman, A., Giorgetta, M. A., Plummer, D., Rozanov, E., Shepherd, T. G., Shibata, K., Stenke, A., Struthers, H., and Tian, W.: Northern winter stratospheric temperature and ozone responses to ENSO inferred from an ensemble of Chemistry Climate Models, Atmos. Chem. Phys., 9, 8935–8948, doi:10.5194/acp-9-8935-2009, 2009.

Cai, W. J. and Cowan, T.: La Niña Modoki impacts Australia autumn rainfall variability, Geophys. Res. Lett., 36, L12805, doi:10.1029/2009GL037885, 2009.

Calvo, F. N., García, R., García Herrera, R., Gallego Puyol, D., Gimeno Presa, L., Hernández Martín, E., and Ribera Rodríguez, P.: Analysis of the ENSO signal in tropospheric and stratospheric temperatures observed by MSU, 1979–2000, J. Climate, 17, 3934–3946, 2004.

Calvo, N., Giorgetta, M. A., Garcia-Herrera, R., and Manzini, E.: Nonlinearity of the combined warm ENSO and QBO effects on the Northern Hemisphere polar vortex in MAECHAM5 simulations, J. Geophys. Res., 114, D13109, doi:10.1029/2008JD011445, 2009.

Camp, C. D. and Tung, K.-K.: Stratospheric polar warming by ENSO in winter: A statistical study, Geophys. Res. Lett., 34, L04809, doi:10.1029/2006GL028521, 2007.

Chandra, S., Ziemke, J. R., Min, W., and Read, W. G.: Effects of 1997–1998 El Niño on tropospheric ozone and water vapor, Geophys. Res. Lett., 25, 3867–3870, 1998.

Deser, C., and Wallace, J. M.: Large-scale atmospheric circulation features associated with warm and cold episodes in thetropical Pacific, J. Climate, 3, 1254–1281, 1990.

Edmon, H. J., Hoskins, B. J., and McIntyre, M. E.: Eliassen-Palm cross-sections for the troposphere, J. Atmos. Sci., 37, 2600–2616 (corrigendum, 38, p. 1115), 1980.

Feng, J. and Li, J.: Influence of El Niño Modoki on spring rainfall over south China, J. Geophys. Res., 116, D13102, doi:10.1029/2010JD015160, 2011.

Free, M. and Seidel, D. J.: The observed ENSO temperature signal in the stratosphere, J.

ACPD
12, 3619–3653, 2012

Geophys. Res., 114, D23108, doi:10.1029/2009JD012420, 2009.
Fueglistaler, S., and Haynes, P. H.: Control of interannual and longer-term variability of stratospheric water vapor, J. Geophys. Res., 110, D24108, doi:10.1029/2005JD006019, 2005.
García-Herrera, R., Calvo, N., Garcia, R. R., and Giorgetta, M. A.: Propagation of ENSO temperature signals into the middle atmosphere: A comparison of two general circulation models and ERA-40 reanalysis data, J. Geophys. Res., 111, D06101, doi:10.1029/2005JD006061, 2006.
Garcia, R. R., Marsh, D. R., Kinnison, D. E., Boville, B. A., and Sassi, F.: Simulation of secular trends in the middle atmosphere, 1950–2003, J. Geophys. Res., 112, D09301, doi:10.1029/2006JD007485, 2007.
Garfinkel, C. I. and Hartmann, D. L.: Effects of El Nino – Southern Oscillation and the Quasi-Biennial Oscillation on polar temperatures in the stratosphere, J. Geophys. Res., 112, D19112, doi:10.1029/2007JD008481, 2007.
Gettelman, A., Randel, W. J., Massie, S., and Wu, F.: El Niño as a Natural Experiment for Studying the Tropicsal Tropopause Region, J. Climate, 14, 3375–3392, 2001.
Gettelman, A., Hegglin, M. I., Son, S.-W., Kim, J., Fujiwara, M., Birner, T., Kremser, S., Rex, M., Anel, J. A., Akiyoshi, H., Austin, J., Bekki, S., Braesike, P., Brühl, C., Butchart, N., Chipperfield, M., Dameris, M., Dhomse, S., Garny, H., Hardiman, S. C., Jöckel, P., Kinnison, D. E., Lamarque, J. F., Mancini, E., Marchand, M., Michou, M., Morgenstern, O., Pawson, S., Pitari, G., Plummer, D., Pyle, J. A., Rozanov, E., Scinocca, J., Shepherd, T. G., Shibata, K., Smale, D., Teyssedre, H., and Tian, W.: Multimodel assessment of the upper troposphere and lower stratosphere: Tropics and global trends, J. Geophys. Res., 115, D00M08, doi:10.1029/2009JD013638, 2010.
Geller, M. A., Zhou, X., and Zhang, M.: Simulations of the interannual variability of stratospheric water vapor, J. Atmos. Sci., 59, 1076–1085, 2002.
Hamilton, K.: An examination of observed Southern Oscillation effects in the Northern Hemisphere stratosphere, J. Atmos. Sci., 50, 3468–3473, 1993.
Hatsushika, H. and Yamazaki, K.: Stratospheric drain over Indonesia and dehydration within the tropicsal tropopause layer diagnosed by air parcel trajectories, J. Geophys. Res., 108, 4610, doi:10.1029/2002JD002986, 2002.
Hitoshi, M. and Hirooka, T.: Predictability of stratospheric sudden warming: A case study for 1998/99 winter, Mon. Weather Rev., 132, 1764–1776, 2004.
Holton, J. R., Haynes, P. H., Douglass, A. R., Rood, R. B., and Pfister, L.:

ACPD
12, 3619–3653, 2012

Stratosphere-troposphere exchange, Rev. Geophys., 33, 403–439, 1995.
Hu, Y. and Tung, K. K.: Interannual and decadal variations of planetary wave activity, stratospheric cooling, and northern hemisphere annular mode, J. Climate, 15, 1659–1673, 2002.
Hurwitz, M. M., Newman, P. A., Oman, L. D., and Molod, A. M.: Response of the Antarctic Stratosphere to Two Types of El Niño Events, J. Atmos. Sci., 68, 812–822, doi:10.1175/2011JAS3606.1, 2011.
Kiladis, G. N., Straub, K. H., Reid, G. C., and Gage, K. S.: Aspects of interannual and intraseasonal variability of the tropopause and lower stratosphere, Q. J. Roy. Meteor. Soc., 127, 1961–1983, 2001.
Manzini, E., Giorgetta, M. A., Esch, M., Kornblueh, L., and Roeckner, E.: The Influence of Sea Surface Temperatures on the Northern Winter Stratosphere: Ensemble Simulations with the MAECHAM5 Model, J. Climate, 19, 3863–3881, 2006.
McCormack, J. P., Fu, R., and Read, W. G.: The influence of convective outflow on water vapor mixing ratios in the tropical upper troposphere: An analysis based on UARS MLS measurements, Geophys. Res. Lett., 27, 525–528, 2000.
Newell, R. E. and Gould-Stewart, S.: A stratospheric fountain?, J. Atmos. Sci., 38, 2789–2796, 1981.
Newell, R. E., Zhu, Y., Browell, E. V., Read, W. G., and Waters, J. W.: Walker circulation and tropical upper tropospheric water vapor, J. Geophys. Res., 101, 1961–1974, doi:10.1029/95JD02275, 1996.
Philander, S. G.: El Niño, La Niña and the Southern Oscillation, Academic Press, 293 pp., 1990.
Randel, W. J.: Study of planetary waves in the southern winter Troposphere and Stratosphere. Part I: wave structure and vertical propagation, J. Atmos. Sci., 44, 917–935, 1987.
Randel, W. J., Wu, F., and Gaffen, D. J.: Interannual variability of the tropicsal tropopause derived from radiosonde data and NCEP reanalysis, J. Geophys. Res., 105, 15509–15523, 2000.
Rasmusson, E. M. and Carpenter, T. H.: Variations in tropical sea surface temperature and surface wind fields associated with the Southern Oscillation/El Niño, Mon. Weather Rev., 110, 354–384, doi:10.1175/1520-0493(1982)110<0354:VITSST>2.0.CO;2, 1982.
Rayner, N. A., Brohan, P., Parker, D. E., Folland, C. K., Kennedy, J. J., Vanicek, M., Ansell, T., and Tett, S. F. B.: Improved analyses of changes and uncertainties in sea surface temperature measured in situ since the mid-nineteenth century: the HadSST2 data set, J. Climate,

ACPD
12, 3619–3653, 2012

19, 446–469, 2006.
Reid, G. C. and Gage, K. S.: Interannual variations in the height of the tropical tropopause, J. Geophys. Res., 90, 5629–5635, 1985.
Reid, G. C., Gage, K. S., and McAfee, J. R.: The thermal response of the tropical atmosphere to variations in equatorial Pacific sea surface temperature, J. Geophys. Res., 94, 14705–14716, 1989.
Sassi, F., Kinnison, D., Boville, B. A., Garcia, R. R., and Roble, R.: Effect of El Niño-Southern Oscillation on the dynamical, thermal, and chemical structure of the middle atmosphere, J. Geophys. Res., 109, D17108, doi:10.1029/2003JD004434, 2004.
Scaife, A. A., Butchart, N., Jackson, D. R., and Swinbank, R.: Can changes in ENSO activity help to explain increasing stratospheric water vapor?, Geophys. Res. Lett., 30, 1880, doi:10.1029/2003GL017591, 2003.
Simmons, A., Uppala, S., and Dee, D.: Update on ERAInterim, ECMWF Newsletter, 111, 5–5, 2007a.
Simmons, A., Uppala, S., Dee, D., and Kobayashi, S.: ERAInterim: New ECMWF reanalysis products from 1989 onwards, ECMWF Newsletter, 110, 25–25, 2007b.
Smith, T. M. and Reynolds, R. W.: Extended reconstruction of global sea surface temperatures based on COADS data (1854–1997), J. Climate, 16, 1495–1510, 2003.
Smith, T. M., Reynolds, R. W., Peterson, T. C., and Lawrimore, J.: Improvements to NOAA's Historical Merged Land Ocean Surface Temperature Analysis (1880–2006), J. Climate., 21, p. 2283, 2008.
SPARC: SPARC Assessment of water vapor in the upper troposphere and lower stratosphere. Stratospheric Processes and Their Role in Climate, WMO/TD-1043, 312 pp., 2000.
Taguchi, M. and Hartmann, D. L.: Increased occurrence of stratospheric sudden warmings during El Nino as simulated by WACCM, J. Climate, 19, 324–332, 2006.
Taschetto, A. S., and England, M. H.: El Niño Modoki impacts on Australian rainfall, J. Climate, 22, 3167–3174, doi:10.1175/2008JCLI2589.1, 2009.
Trenberth, K. E.: The definition of El Niño, B. Am. Meteorol. Soc., 78, 2771–2777, doi:10.1175/1520-0477(1997)078<2771:TDOENO>2.0.CO;2, 1997.
Trenberth, K. E. and Smith, L.: The vertical structure of temperature in the tropics: Different flavors of El Niño, J. Climate, 19, 4956–4970, 2006.
Trenberth, K. E. and Smith, L.: Variations in the three-dimensional structure of the atmospheric circulation with different flavors of El Niño, J. Climate, 22, 2978–2991, 2009.

ACPD
12, 3619–3653, 2012

Trenberth, K. E. and Stepaniak, D. P.: Indices of El Niño evolution, J. Climate, 14, 1697–1701, 2001.
Uppala, S., Dee, D., Kobayashi, S., Berrisford, P. and Simmons, A.: Towards a climate data assimilation system:status update of ERA-Interim, ECMWF Newsletter, 115, 12–18, 2008.
Van Loon, H. and Labitzke, K.: The Southern Oscillation. Part V: The anomalies in the lower stratosphere of the Northern Hemisphere in winter and a comparison with the quasi-biennial oscillation, Mon. Weather Rev., 115, 357–369, 1987.
Weng, H. Y., Karumuri, A., Swadhin, K. B., Suryachandra, A. R., and Toshio, Y.: Impacts of recent El Niño Modoki on dry/wet conditions in the Pacific rim during boreal summer, Clim. Dynam., 29, 113–129, doi:10.1007/s00382-007-0234-0, 2007.
Weng, H. Y., Behera, S. K., and Yamagata, T.: Anomalous winter climate conditions in the Pacific rim during recent El Niño Modoki and El Niño events, Clim. Dynam., 32, 663–674, doi:10.1007/s00382-008-0394-6, 2009.
World Meteorological Organization: Scientific Assessment of Ozone Depletion: 2002, WMO Global Ozone Research and Monitoring Project-Report No. 47, Geneva, Switzeland, 2003.
Xie, F., Tian, W., Austin, J., Li, J., Tian, H., Shu, J., and Chen, C.: The effect of ENSO activity on lower stratospheric water vapor, Atmos. Chem. Phys. Discuss., 11, 4141–4166, doi:10.5194/acpd-11-4141-2011, 2011.
Yulaeva, E., Holton, J. R., and Wallace, J. M.: On the cause of the annual cycle in the tropical lower stratospheric temperature, J. Atmos. Sci., 51, 169–174, 1994.
Zhang, W. J., Li, J. P., and Jin, F. F.: Spatial and temporal features of ENSO meridional scales, Geophys. Res. Lett., 36, L15605, doi:10.1029/2009GL038672, 2009.
Zhang, W. J., Li, J. P., and Zhao, X.: Sea surface temperature cooling mode in the Pacific cold tongue, J. Geophys. Res., 115, C12042, doi:10.1029/2010JC006501, 2010.
Zhou, T. J. and Zhang, J.: The Vertical Structures of Atmospheric Temperature Anomalies Associated with Two Flavors of El Nino Simulated by AMIP II Models, J. Climate, 24, 1053–1070, doi:10.1175/2010JCLI3504.1, 2010.

ACPD
12, 3619–3653, 2012

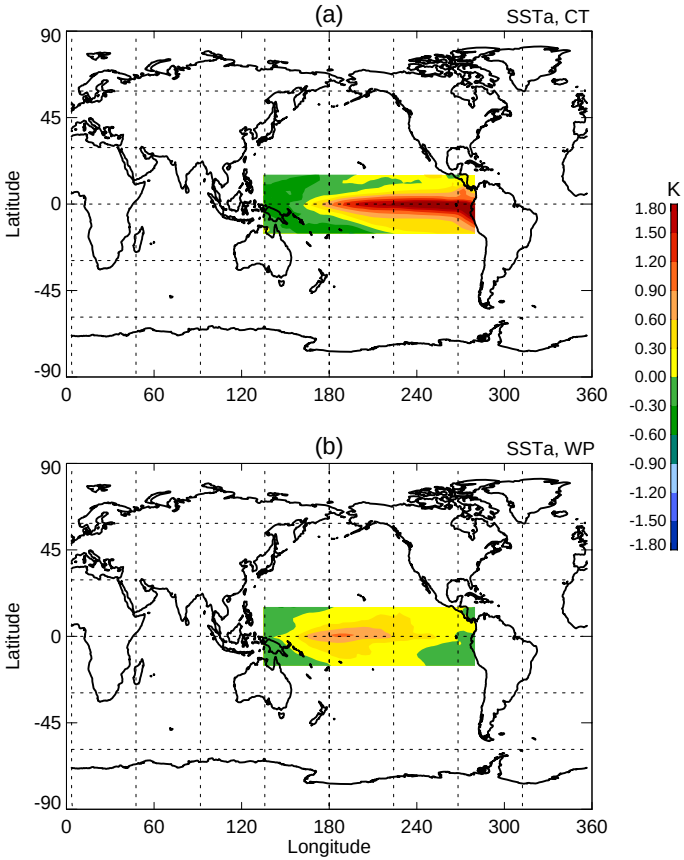

Fig. 1. SSTAs in the tropical Pacific Ocean referred to as canonical El Niño events **(a)** and El Niño Modoki events **(b)**. The logogram CT on the top right corner of a panel represents the canonical El Niño events. The logogram of WP represents the El Niño Modoki events. CT and WP in the following figures have the same meaning.

ACPD
12, 3619–3653, 2012

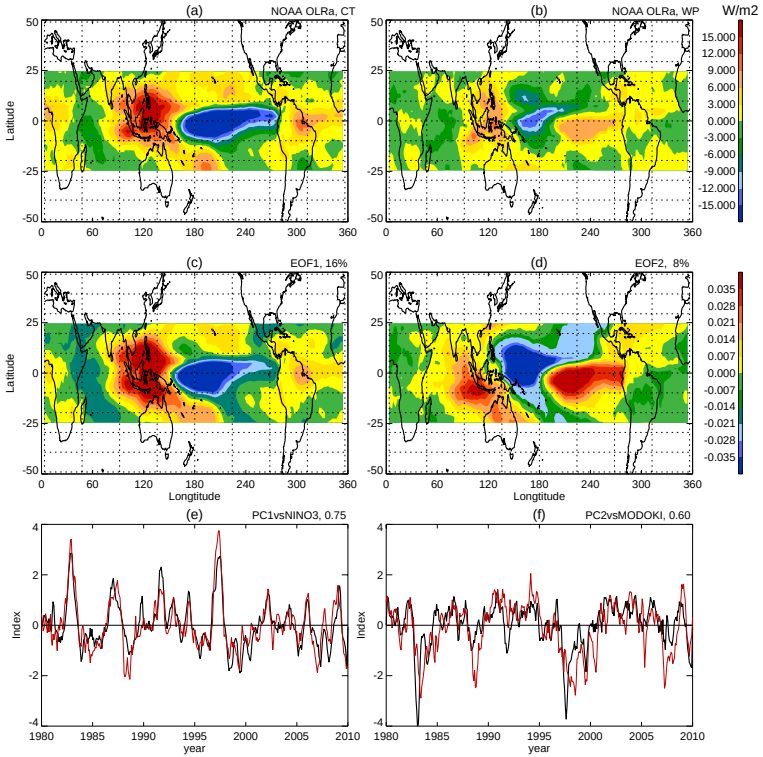

Fig. 2. Composited OLR anomalies for **(a)** canonical El Niño events, and **(b)** El Niño Modoki events, based on NOAA data for 1979–2010. Contour interval, $3\,W\,m^{-2}$. **(c)** and **(d)** are the leading and second modes of the EOF spatial pattern of OLR anomalies, respectively. Contour interval, 0.007. **(e)** and **(f)** are the leading and second modes of PC interannual variability, respectively. The red line in **(e)** is the N3I; the red line in **(f)** is the EMI. The values at the top right corners of **(e)** and **(f)** are correlation coefficients describing the correlations between the datasets.

ACPD
12, 3619–3653, 2012

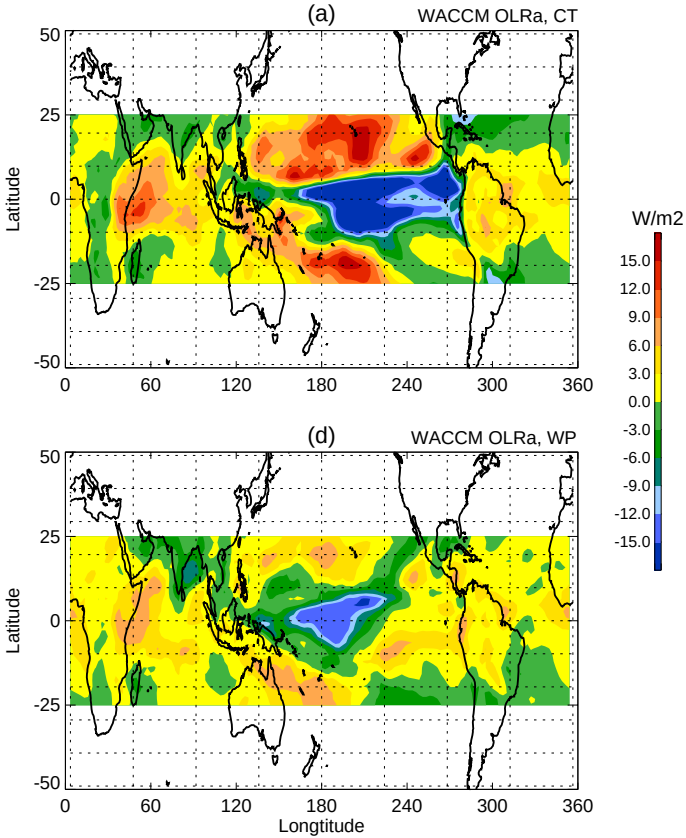

Fig. 3. Averaged OLR anomalies for R2-R1 **(a)** and R3-R1 **(b)**. Contour interval, 3 W m^{-2}.

ACPD
12, 3619–3653, 2012

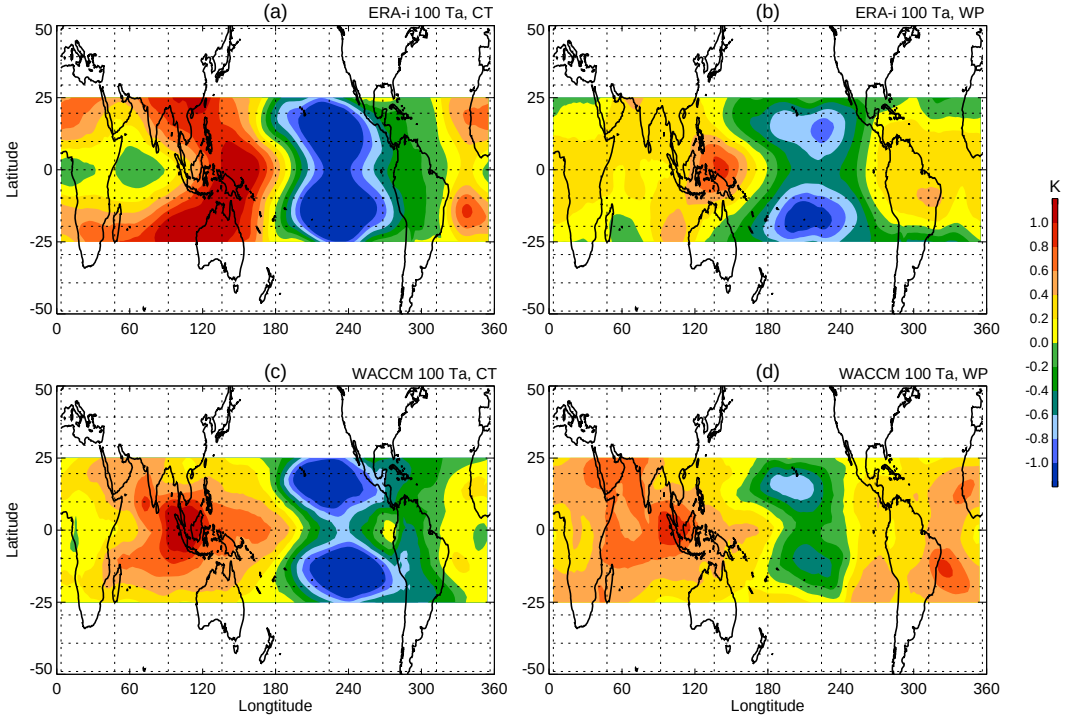

Fig. 4. Composite temperature anomalies at 100 hPa for **(a)** canonical El Niño events and **(b)** El Niño Modoki events, based on ERA-Interim data for 1979–2010. Temperature anomalies at 100 hPa for R2-R1 **(c)** and R3-R1 **(d)**. Contour interval, 0.2 K.

ACPD
12, 3619–3653, 2012

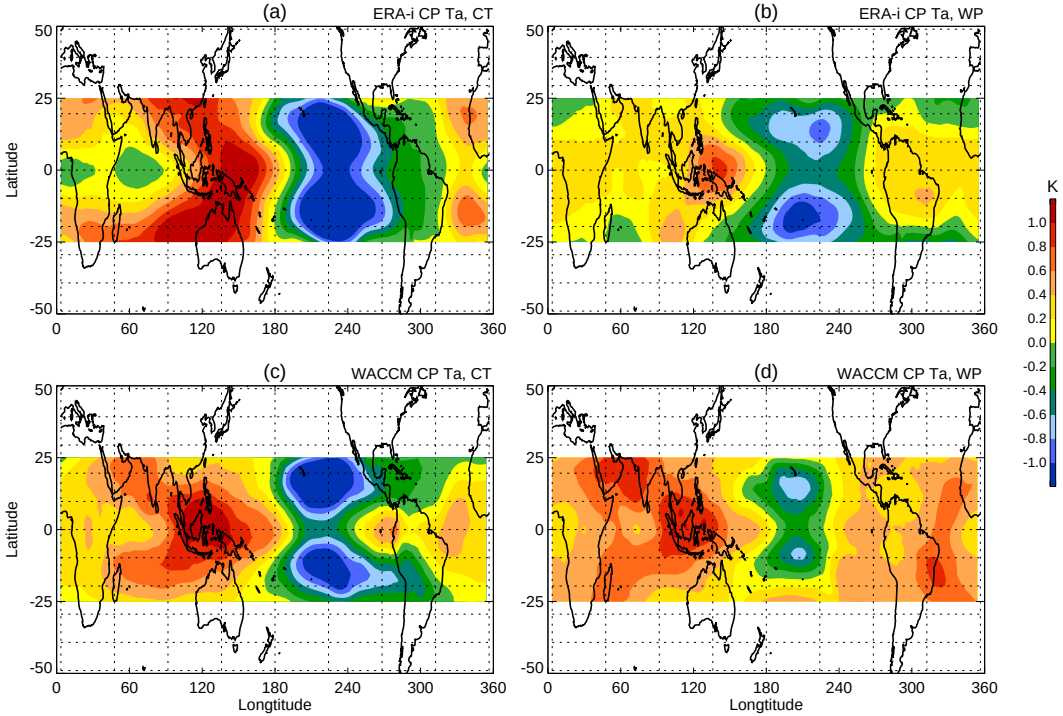

Fig. 5. Cold point temperature anomalies in the tropopause based on composite ERA-Interim data, 1979–2010: **(a)** canonical El Niño events, and **(b)** El Niño Modoki events. Anomalies in cold point tropopause temperatures, for R2-R1 **(c)** and R3-R1 **(d)**. Contour intervals, 0.2 K.

ACPD
12, 3619–3653, 2012

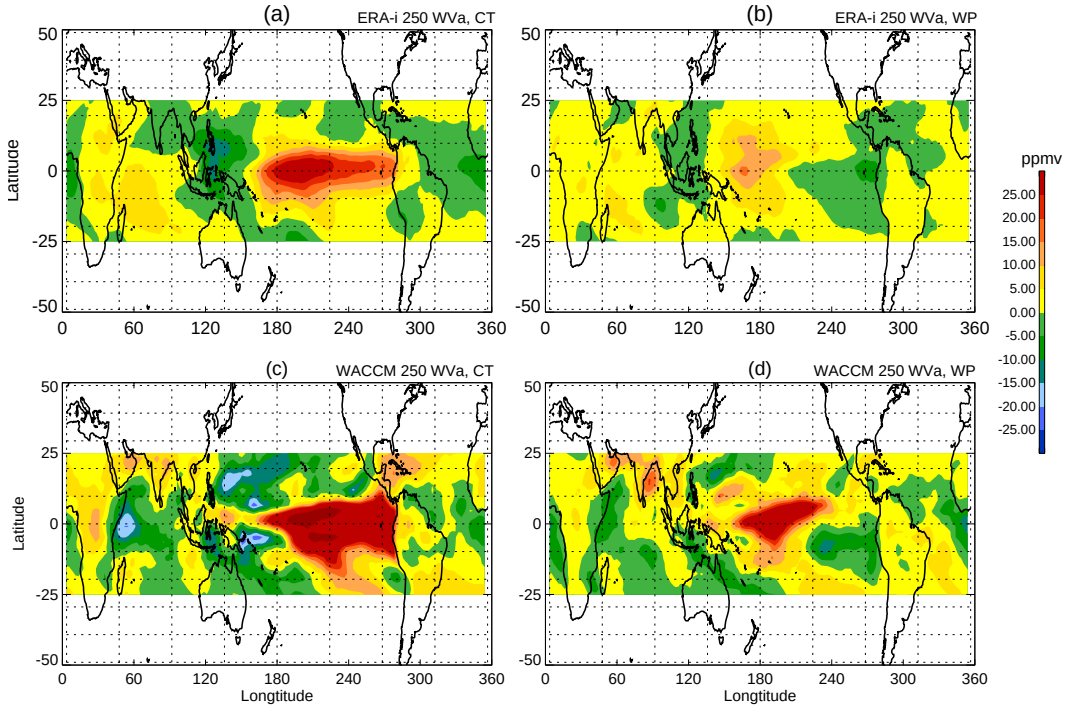

Fig. 6. Water vapor anomalies at 250 hPa based on composite ERA-Interim data, 1979–2010: **(a)** canonical El Niño events and **(b)** El Niño Modoki events. Water vapor anomalies at 250 hPa for R2-R1 **(c)** and R3-R1 **(d)**. Contour intervals, ±5 ppm water vapor.

ACPD
12, 3619–3653, 2012

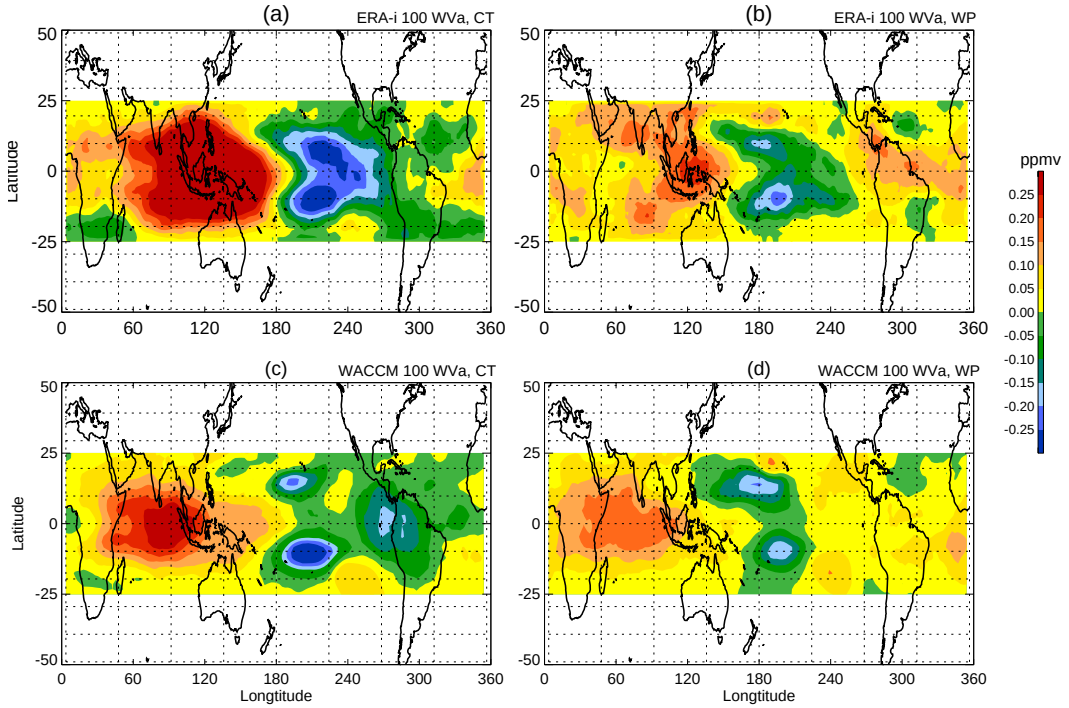

Fig. 7. Water vapor anomalies at 100 hPa based on composite ERA-Interim data, 1979–2010: **(a)** canonical El Niño events and **(b)** El Niño Modoki events. Water vapor anomalies at 100 hPa for R2-R1 **(c)** and R3-R1 **(d)**. Contour intervals, 0.05 ppm water vapor.

ACPD
12, 3619–3653, 2012

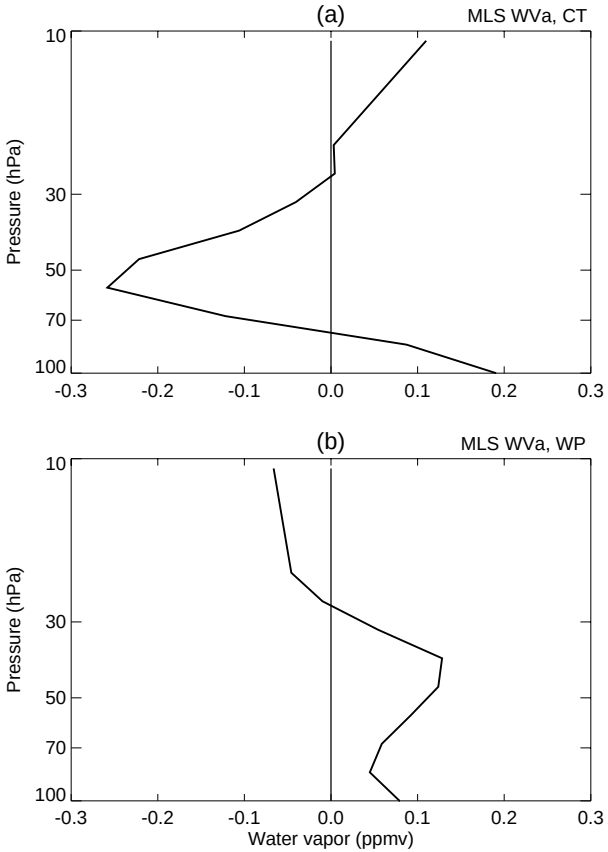

Fig. 8. Vertical profiles of averaged composite zonal mean water vapor concentration anomalies in the tropics (25° S–25° N) based on ERA-Interim data for **(a)** canonical El Niño events and **(b)** El Niño Modoki events.

ACPD
12, 3619–3653, 2012

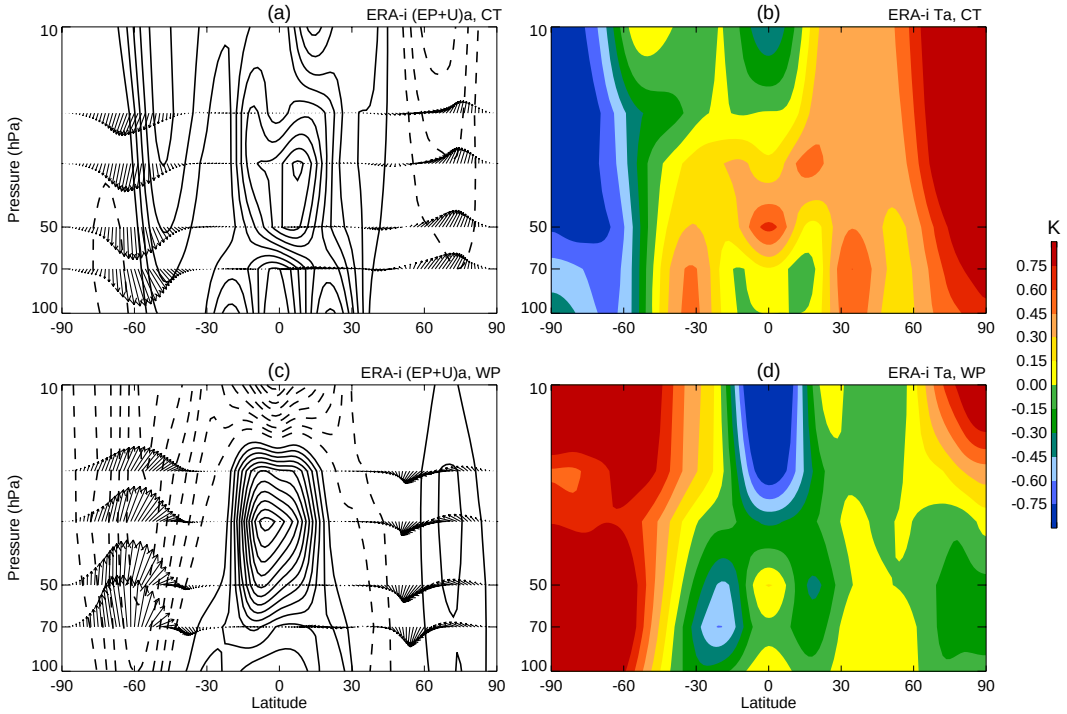

Fig. 9. Composite anomalies of the E-P flux and zonal wind for **(a)** canonical El Niño events and **(c)** El Niño Modoki events, based on ERA-Interim data for 1979–2010. The unit horizontal vector is 10^7 kg s^{-1} and the unit vertical vector is 10^5 kg s^{-1}. The contour interval for zonal wind anomalies is 0.4 m s^{-1}. Solid and dashed lines in **(a)** and **(c)** represent positive and negative zonal wind anomalies, respectively. Composite anomalies of temperature for **(b)** canonical El Niño events and **(d)** El Niño Modoki events, based on ERA-Interim data for 1979–2010. Contour interval for temperature anomalies, 0.15 K.

ACPD
12, 3619–3653, 2012

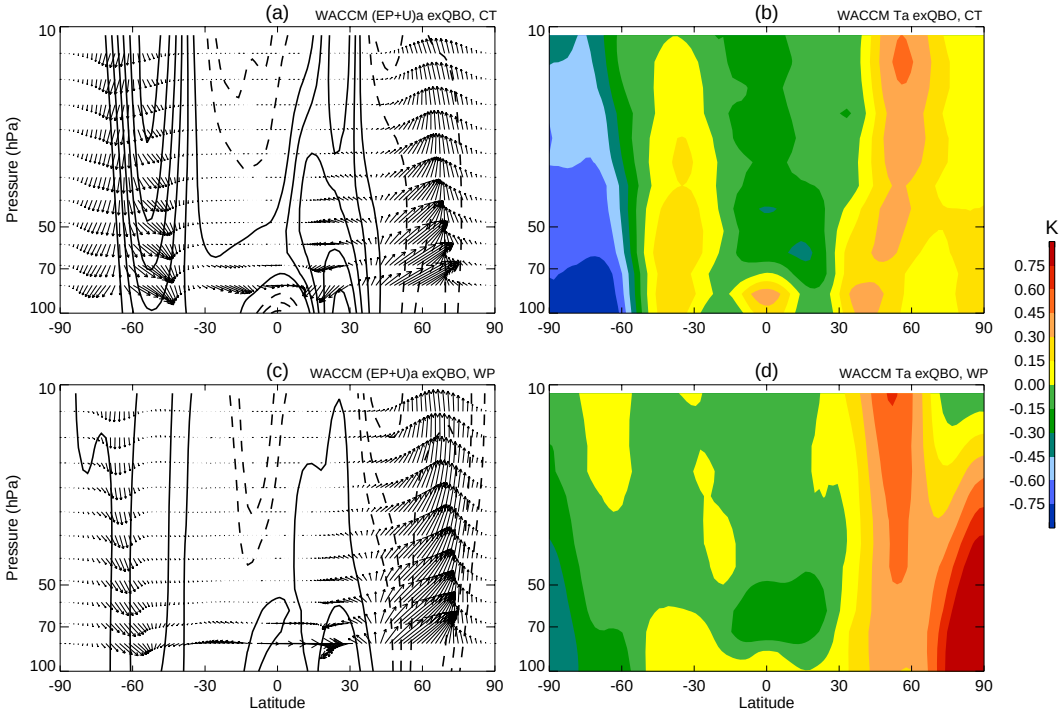

Fig. 10. Same as Fig. 9, but for R2-R1 (**a** and **b**) and R3-R1 (**c** and **d**).

ACPD
12, 3619–3653, 2012

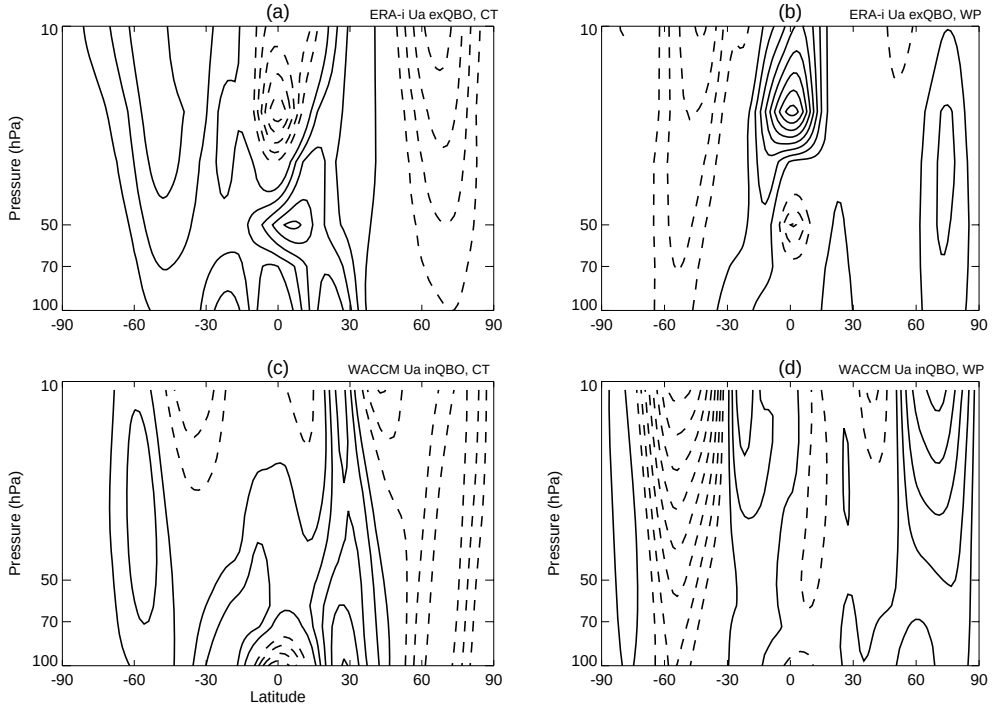

Fig. 11. Composite anomalies of the zonal wind for **(a)** canonical El Niño events and **(b)** El Niño Modoki events, obtained using filtered ERA-Interim data (see text for details). Anomalies of the zonal wind for **(c)** canonical El Niño events and **(d)** El Niño Modoki events, obtained from WACCM3 include QBO (see text for details). Contour interval for zonal wind anomalies, $0.4\,\mathrm{m\,s^{-1}}$.

ACPD
12, 3619–3653, 2012